LETTER

doi:10.1038/nature10772

Extrathymically generated regulatory T cells control mucosal T_H2 inflammation

Steven Z. Josefowicz[1,2]*, Rachel E. Niec[1]*, Hye Young Kim[3], Piper Treuting[4], Takatoshi Chinen[1,5], Ye Zheng[6], Dale T. Umetsu[3] & Alexander Y. Rudensky[1]

A balance between pro- and anti-inflammatory mechanisms at mucosal interfaces, which are sites of constitutive exposure to microbes and non-microbial foreign substances, allows for efficient protection against pathogens yet prevents adverse inflammatory responses associated with allergy, asthma and intestinal inflammation[1]. Regulatory T (T_{reg}) cells prevent systemic and tissue-specific autoimmunity and inflammatory lesions at mucosal interfaces. These cells are generated in the thymus (tT_{reg} cells) and in the periphery (induced (i)T_{reg} cells), and their dual origin implies a division of labour between tT_{reg} and iT_{reg} cells in immune homeostasis. Here we show that a highly selective blockage in differentiation of iT_{reg} cells in mice did not lead to unprovoked multi-organ autoimmunity, exacerbation of induced tissue-specific autoimmune pathology, or increased pro-inflammatory responses of T helper 1 (T_H1) and T_H17 cells. However, mice deficient in iT_{reg} cells spontaneously developed pronounced T_H2-type pathologies at mucosal sites—in the gastrointestinal tract and lungs—with hallmarks of allergic inflammation and asthma. Furthermore, iT_{reg}-cell deficiency altered gut microbial communities. These results suggest that whereas T_{reg} cells generated in the thymus appear sufficient for control of systemic and tissue-specific autoimmunity, extrathymic differentiation of T_{reg} cells affects commensal microbiota composition and serves a distinct, essential function in restraint of allergic-type inflammation at mucosal interfaces.

Exquisitely balanced control mechanisms operating at mucosal sites are able to accommodate potent immune defences and the need to prevent tissue damage resulting from inflammatory responses caused by commensal microorganisms, food and environmental antigens, allergens, and noxious substances[1].

Prominent among multiple regulatory lymphoid and myeloid cell subsets operating at environmental interfaces are $Foxp3^+$ T_{reg} cells. Genetic deficiency in Foxp3 (forkhead box P3, a key transcription factor specifying T_{reg} cell differentiation) leads to paucity of $Foxp3^+$ T_{reg} cells and consequent generalized lympho- and myelo-proliferative syndrome, featuring sharply augmented serum IgE levels, production of T_H1, T_H2 and T_H17 cytokines, and widespread tissue inflammation[2]. Foxp3 can be induced in thymocytes in response to T-cell receptor (TCR) and CD28 stimulation, and IL-2. In addition, Foxp3 can be upregulated upon TCR stimulation of mature peripheral $CD4^+$ T cells in the presence of tumour growth factor β (TGFβ) in a manner dependent on an intronic *Foxp3* enhancer CNS1 (refs 3–5). Inflammatory cytokines and potent co-stimulatory signals antagonize the peripheral induction of Foxp3, and retinoic acid augments Foxp3 induction through mitigating inflammatory cytokine production and through cell intrinsic mechanisms[1,6–8]. Although differing in their sites of generation, tT_{reg} and iT_{reg} cells are comingled in the secondary lymphoid organs and non-lymphoid tissues once mature, and their relative contributions to the total population of T_{reg} cells and their specific roles in control of various aspects of immune homeostasis and microbial colonization in normal animals has remained unexplored.

Our recent investigation[5] showed that CNS1, which contains binding sites for transcription factors (NFAT, Smad3 and RAR/RXR) downstream of three signalling pathways implicated in iT_{reg} cell generation[4,8] (Supplementary Fig. 1), is critical for TGFβ-dependent induction of Foxp3, but has no apparent role in tT_{reg} differentiation or maintenance of Foxp3 expression. This observation suggested that CNS1 activity represents a dedicated genetic determinant for the differentiation of iT_{reg} cells, and its deficiency in mice provides a unique means to evaluate the function of these cells *in vivo*. Our initial characterization of $CNS1^-$ mice and littermates maintained on a 129/B6 genetic background failed to reveal disease phenotypes. Because mixed genetic backgrounds frequently mask adverse phenotypes or make them highly variable, to understand iT_{reg} function *in vivo* we backcrossed CNS1 mice onto the B6 background (Supplementary Fig. 2).

First, we sought to ascertain that on the B6 genetic background CNS1 is dispensable for tT_{reg} cell generation but critical for generation of iT_{reg} cells. Two recent studies established a role for TGFβ signalling in tT_{reg} cell differentiation in neonates[9,10]. Thus, to exclude the possibility that CNS1 deficiency adversely affects generation of $Foxp3^+$ T cells in the neonatal thymus, we examined the $Foxp3^+$ T_{reg} cell population in heterozygous female $CNS1^{WT/-}$ mice. As Foxp3 is encoded on the X chromosome and is subject to random X-chromosome inactivation, characterization of female $CNS1^{WT/-}$ mice allows for comparison of $CNS1^-$ and $CNS1^{WT}$ T_{reg} cells in a competitive environment. In neonatal female $CNS1^{WT/-}$ mice, $CNS1^-$ cells constituted, on average, one-half of the thymic $Foxp3^+$ cell population (Fig. 1a). Additionally, neonatal $CNS1^-$ hemizygous and control males harboured comparable numbers of $Foxp3^+$ thymocytes (Supplementary Fig. 3). Therefore, tT_{reg} differentiation is independent of CNS1. In contrast, $CNS1^-$ naive CD4 T cells showed severely impaired induction of Foxp3 *in vitro* (Fig. 1b). Analyses of heterozygous female $CNS1^{WT/-}$ mice and transfer of $CNS1^-$ or $CNS1^{WT}$ T_{reg} cells into lymphopenic recipients demonstrated that the ability of T_{reg} cells to accumulate and proliferate in various tissues was unperturbed in the absence of CNS1 (Supplementary Fig. 4). Furthermore, CNS1 deficiency did not affect suppressor activity of tT_{reg} cells (assessed using *in vitro* suppression assays and adoptive transfers of Foxp3-deficient effector T cells with predominantly tT_{reg}-containing $Foxp3^+$ cells isolated from 4-week-old $CNS1^-$ and $CNS1^{WT}$ mice into lymphopenic recipients (Supplementary Fig. 5)). Likewise, CNS1 ablation did not negatively affect maintenance of Foxp3 expression and overall function of NFAT, TGFβ and retinoic acid signalling pathways in these cells (Supplementary Fig. 5 and data not shown). To assess how the deficiency in iT_{reg} cell generation affects the size of the peripheral T_{reg} cell compartment, we analysed T_{reg} cell frequencies in various tissues throughout the lifespan of mice. $CNS1^-$ mice failed to exhibit a progressive age-dependent increase in $Foxp3^+$

[1]Howard Hughes Medical Institute and Immunology Program, Sloan Kettering Institute, New York, New York 10021, USA. [2]Laboratory of Chromatin Biology and Epigenetics, The Rockefeller University, New York, New York 10065, USA. [3]Division of Immunology, Children's Hospital, Harvard Medical School, Boston, Massachusetts 02115, USA. [4]Department of Comparative Medicine, and Histology and Imaging Core, School of Medicine, University of Washington, Seattle, Washington 98195, USA. [5]Department of Microbiology and Immunology, Keio University School of Medicine, Tokyo 160-8582, Japan. [6]Nomis Foundation Laboratories for Immunobiology and Microbial Pathogenesis, Salk Institute for Biological Studies, La Jolla, California 92037, USA.
*These authors contributed equally to this work.

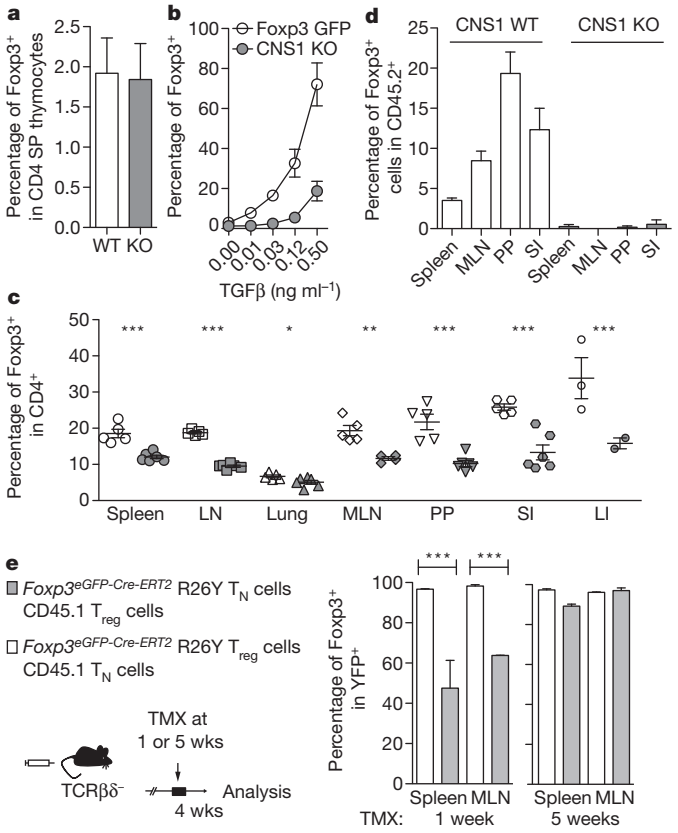

Figure 1 | Impaired iT$_{reg}$ cell generation and altered composition of the peripheral T$_{reg}$ cell population in CNS1-deficient mice. **a**, Relative contribution of CNS1^{-} (GFP^{+}) and CNS1^{WT} (GFP^{-}) cells to the Foxp3^{+} thymocyte subset in 4-day-old *CNS1*$^{WT/-}$ female mice. SP, single positive. **b**, Induction of Foxp3 in Foxp3^{-} T$_{N}$ (naive) cells FACS sorted from CNS1^{-} (knockout, KO) or *Foxp3*^{GFP} mice stimulated *in vitro* with TGFβ, IL-2 anti-CD3 and anti-CD28. **c**, Percentage of Foxp3^{+} cells (of CD4^{+}) in the spleen, lymph node (LN), mesenteric lymph nodes (MLN), Peyer's patches (PP) and cells from the small and large intestine lamina propria (SI and LI) of 6–9 month old CNS1^{-} or control mice. **d**, Percentage of transferred (CD45.2^{+}) CNS1^{-} or CNS1^{+} CD25^{-}CD44^{low}CD45.2^{+}OTII^{+} cells that induced Foxp3 following administration of OVA in water for 6 days. **e**, Stability of Foxp3 expression in iT$_{reg}$ cells. FACS sorted GFP^{+} or GFP^{-} cells from *Foxp3*$^{eGFP\text{-}Cre\text{-}ERT2}$ mice were transferred with GFP^{-} or GFP^{+} cells, respectively, from CD45.1 *Foxp3*^{GFP} mice into TCRβδ-deficient recipients. Mice received tamoxifen (TMX) at 1 (left) or 5 weeks (right) after transfer and stability of Foxp3 expression among YFP-labelled cells was assessed after 4 weeks. All data are representative of two or more independent experiments with $n \geq 3$. Error bars, s.d.; $^{*}P < 0.05$, $^{**}P < 0.01$, $^{***}P < 0.001$, as calculated by Students' *t*-test.

cell frequencies observed in wild-type littermates (Fig. 1c and Supplementary Fig. 6). By 6–8 months of age, CNS1^{-} mice contained markedly fewer Foxp3^{+} cells in comparison to control animals, with most prominent differences in mesenteric lymph nodes, Peyer's patches, and small and large intestine lamina propria, sites known to support iT$_{reg}$ cell generation[11]. This trend was not the result of expression of a Foxp3–GFP fusion protein in CNS1^{-} mice, because age-matched CNS1^{WT} Foxp3–GFP and littermate control CNS1^{WT} mice expressing unmodified Foxp3 protein exhibited similar age-dependent increases in T$_{reg}$ cell frequencies (Supplementary Fig. 6).

To assess the extent of impairment of peripheral generation of T$_{reg}$ cells *in vivo*, we examined Foxp3 induction in antigen-specific naive T cells upon exposure to ingested 'non-self' antigen[12]. Ovalbumin (OVA)-specific OT-II^{+} TCR-transgenic Foxp3^{-} (GFP^{-}) T$_{reg}$ cells from CNS1^{-} or *Foxp3*^{GFP} mice were transferred into CD45.1^{+} lymphoreplete recipients followed by *ad libitum* administration of OVA in drinking water. We failed to detect Foxp3 induction in CNS1-deficient cells, whereas up to 20% of transferred OT-II T cells from control *Foxp3*^{GFP} mice induced Foxp3 upon exposure to cognate antigen in the intestinal tract (Fig. 1d and Supplementary Fig. 7). These results were in agreement with a marked impairment in Foxp3 induction in polyclonal CNS1-deficient Foxp3^{-} T cells *in vitro*, which was most severe at lower, more physiologically relevant concentrations of TGFβ (Fig. 1b). Together these data indicate that iT$_{reg}$ cells have a stringent requirement for CNS1 for their differentiation.

Recent studies showed a limited TCR-dependent clonal niche for tT$_{reg}$ cell differentiation and peripheral maintenance[13–15]. The sustained numerical impairment in the peripheral T$_{reg}$ cell populations in CNS1-deficient mice suggests that tT$_{reg}$ cells fail to fill the 'void' in the peripheral T$_{reg}$ cell pool, left by iT$_{reg}$ cell deficiency. This observation combined with largely non-overlapping TCR repertoires of tT$_{reg}$ and iT$_{reg}$ cells suggests that iT$_{reg}$ and tT$_{reg}$ cells occupy distinct 'niches'[16]. To test this notion we co-transferred CNS1^{-} (tT$_{reg}$ cells) or CNS1^{WT} T$_{reg}$ cells (iT$_{reg}$ + tT$_{reg}$) from aged mice with CNS1-sufficient naive CD45.1^{+}Foxp3^{-}CD4^{+} T cells into lymphopenic recipients. We observed more efficient Foxp3 induction in CD45.1^{+}CD4^{+} T cells upon co-transfer with CNS1^{-} T$_{reg}$ cells (tT$_{reg}$ cells), indicating that in lymphopenic recipients the *de novo* generation of iT$_{reg}$ cells is markedly more efficient in the absence of pre-existing iT$_{reg}$ cells (Supplementary Fig. 8). These data also imply the existence of a stable iT$_{reg}$ cell subset in normal mice. However, the dynamics and stability of Foxp3 expression has been a controversial issue, with a number of studies favouring unstable Foxp3 expression in iT$_{reg}$ cells[17–19]. Thus, we next employed genetic fate mapping using inducible Cre recombinase expressed in a T$_{reg}$-specific manner (*Foxp3*$^{EGFP\text{-}CRE\text{-}ERT2}$) and a Rosa26–YFP recombination reporter allele (R26Y)[20] to determine if iT$_{reg}$ cells generated *in vivo* are able to acquire stable Foxp3 expression and, thus, have the capacity to contribute to the stable T$_{reg}$ cell compartment.

Double-sorted naive CD45.2^{+}Foxp3^{-}YFP^{-} CD4 T cells from *Foxp3*$^{EGFP\text{-}CRE\text{-}ERT2}$ R26Y mice were transferred together with congenically marked CD45.1^{-}Foxp3^{+} T$_{reg}$ cells into lymphopenic recipient mice. Foxp3 expression within the population of tagged YFP^{+} cells generated from YFP^{-}Foxp3^{-} precursors was assessed four weeks after treatment of recipient mice with tamoxifen, which was administered early (one week) and late (five weeks) following cell transfer. Approximately half of the newly generated YFP-tagged iT$_{reg}$ cells lost Foxp3 expression, whereas 'mature' iT$_{reg}$ cells tagged at a later time point displayed remarkable stability (>90% Foxp3^{+} cells among YFP^{+} cells), comparable to that of transferred peripheral T$_{reg}$ cells (Fig. 1e and Supplementary Fig. 9). Together these data indicate that iT$_{reg}$ cells have a stringent requirement for CNS1 for their differentiation, accumulate throughout life, and occupy a sizable fraction of the stable peripheral T$_{reg}$ cell compartment.

CNS1^{-} mice on the B6 genetic background displayed neither early- nor late-onset systemic autoimmunity nor spontaneous widespread tissue lesions nor severe morbidity associated with systemic T$_{reg}$ cell deprivation (data not shown). However, it was possible that iT$_{reg}$ cell deficiency may exacerbate initial or late stages of provoked tissue-specific autoimmune pathology directed against a self-antigen. To address this question, we induced experimental autoimmune encephalomyelitis (EAE) in CNS1-deficient or littermate control mice through immunization with myelin oligodendrocyte glycoprotein (MOG) peptide. The onset, severity and remission of disease were indistinguishable, and no detectable differences were observed in T$_{reg}$ cell subsets in the brain in these two groups of mice (Supplementary Fig. 10). Although it will be important to evaluate the role of iT$_{reg}$ cells in additional models of induced autoimmunity, these results indicate that tT$_{reg}$ cells are largely sufficient for control of tolerance to self-antigens and that the distinct functional role of iT$_{reg}$ cells might be to control inflammation at mucosal surfaces, which are sites of preponderant exposure to non-self substances. This notion is consistent with data indicating that tT$_{reg}$ cells arise from a subset of thymocytes, which exhibit TCR with an increased affinity for self-antigens yet insufficient for negative selection[10,21], whereas iT$_{reg}$ cells are efficiently generated

upon TCR engagement with a high affinity cognate ligand under subimmunogenic conditions[22,23].

The absence of iT$_{reg}$ cell induction in response to oral antigen in CNS1^{-} mice suggested that the immune balance in the gastrointestinal tract might be impaired owing to deficiency in gut antigen-specific iT$_{reg}$ cells. Indeed, while IL-17 and IFN-γ production by CD4^{+} T cells was unaffected by iT$_{reg}$ deficiency in CNS1^{-} mice (Supplementary Fig. 11), we observed markedly augmented production of the T$_H$2 cytokines, IL-4, IL-5 and IL-13, by CD4^{+} T cells, especially in the mesenteric lymph nodes, Peyer's patches and intestinal lamina propria (Fig. 2a and Supplementary Fig. 12). Furthermore, the vast majority of CD4^{+} T cells in the lamina propria of CNS1^{-} mice expressed high amounts of Gata3, a key T$_H$2 differentiation factor. Increases in Gata3^{+}CD4^{+} T cells were observed not only in gastrointestinal tract tissues in CNS1^{-} mice but also in other lymphoid tissues, albeit to a lesser extent (Fig. 2b and Supplementary Fig. 12). Consistent with the sharply augmented T$_H$2 responses at mucosal sites, CNS1^{-} mice exhibited increased frequencies of germinal centre B cells (Fas^{+}GL7^{+}) in the Peyer's patches, but not in the spleen or peripheral lymph nodes (Supplementary Fig. 13), and spontaneous increases in serum levels of IgE and IgA, but not in other Ig isotypes (Fig. 2c, and data not shown).

The dysregulated T$_H$2 responses were associated with a decreased body weight (Fig. 3a and Supplementary Fig. 2) and distinct highly penetrant pathology throughout the gastrointestinal tract (Fig. 3b and Supplementary Fig. 14): all CNS1^{-} mice (12/12) and no CNS1^{WT} control littermates (0/6) were affected by gastritis and plasmacytic enteritis characterized by increased frequencies of plasma cells in the intestinal lamina propria and other associated lesions such as crypt abscesses. Accordingly, serum antibodies in CNS1^{-} mice exhibited reactivity against antigens of the small and large intestine, pancreas and chow (Supplementary Fig. 13). Notably, the pathology observed in the gastrointestinal tissue of CNS1^{-} mice was markedly diminished upon B-cell depletion, but was not ameliorated by administration of IL-4 neutralizing antibody (Supplementary Fig. 15). The inflammatory features and lesions observed in CNS1^{-} mice were consistent with allergic T$_H$2-type intestinal disease (Fig. 3).

One possible explanation for the pronounced T$_H$2 responses and intestinal pathology associated with iT$_{reg}$ cell deficiency is simply a numerical decrease in T$_{reg}$ cells. However, we consider this possibility unlikely, because graded depletion of Foxp3^{+} T$_{reg}$ cells in Foxp3^{DTR} mice upon administration of titrated amounts of diphtheria toxin resulting in T$_{reg}$ frequencies similar to those observed in CNS1^{-} mice revealed augmented T$_H$1 and T$_H$17, but not T$_H$2, responses[24]. Alternatively, certain qualitative features of iT$_{reg}$ cells could allow them to efficiently limit T$_H$2 inflammation in the gut. Recent studies suggested that some of the transcriptional regulators involved in a particular type of effector T-cell response facilitate the ability of T$_{reg}$ cells to suppress those responses[25–27]. Thus, we explored the expression of T$_H$2-associated transcription factor Gata3 in T$_{reg}$ cells in CNS1^{-} and CNS1^{WT} mice. In contrast to a sharp increase in Gata3 expression in effector T cells (Fig. 2b and Supplementary Fig. 12), we found its expression markedly diminished in T$_{reg}$ cells in CNS1^{-} mice (Fig. 3c and Supplementary Fig. 12). Notably, ablation of a conditional Gata3 allele in T$_{reg}$ cells leads to T$_{reg}$ cell dysfunction[28,29] and marked augmentation of T$_H$2 cytokine production by CD4^{+} T cells (D. Rudra, R.E.N. and A.Y.R., manuscript in preparation). We hypothesized that increased Gata3 expression in iT$_{reg}$ cells reflects their activation state upon TCR ligation by high affinity ligands in the gut rather than an intrinsic feature of iT$_{reg}$ cells. In support of this idea, we found that both CNS1^{-} and control T$_{reg}$ cells stimulated *in vitro* through the TCR and IL-2 receptor exhibited similarly robust Gata3 induction (Supplementary Fig. 12). Thus, we suggest that increased Gata3 expression in iT$_{reg}$ cells, a likely consequence of their generation in response to high affinity TCR ligands present in the gut, endows these cells with the capacity to efficiently control spontaneous mucosal T$_H$2 inflammation.

Certain commensal bacteria increase the frequencies of T$_{reg}$ cells in the gut and provide antigens recognized by a considerable proportion of iT$_{reg}$ TCR[1,16]. In addition to TCR ligands the gut microbial community

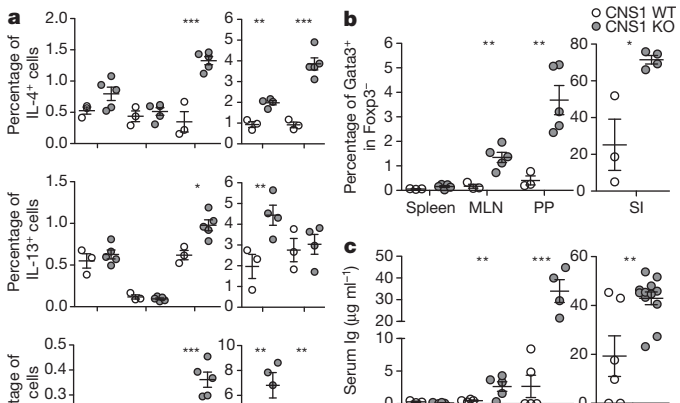

Figure 2 | Paucity of iT$_{reg}$ cells results in T$_H$2 inflammation in the gastrointestinal tract. **a**, Percentage of CD4^{+} cells producing IL-4 (top), IL-13 (middle) and IL-5 (bottom) in 3-month-old mice. Left, spleen, peripheral lymph nodes (LN) and mesenteric lymph nodes (MLN); right, lamina propria of small and large intestine (SI and LI, respectively). **b**, Percentage of Foxp3^{-} CD4^{+} cells that were Gata3^{+} in 3-month old mice (PP, Peyer's patches). **c**, Concentration of IgE and IgA in serum, determined by enzyme linked immunosorbent assay (ELISA) at 1, 3 and 10 months. All data are representative of three or more independent experiments with ≥3 mice per group. Error bars, s.d.; *$P < 0.05$, **$P < 0.01$, ***$P < 0.001$, as calculated by Students' *t*-test.

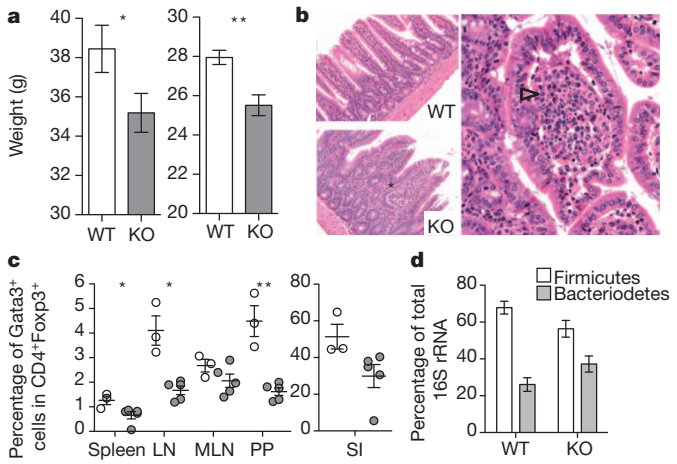

Figure 3 | iT$_{reg}$ cell deficiency leads to T$_H$2 type gastrointestinal pathology and altered microbial communities. **a**, Body weights of 9–12 (left) or 2.5-month-old individually housed (right) CNS1^{-} (KO) and littermate control (WT) mice ($n \geq 12$). **b**, Plasmacytic enteritis (arrowhead) in CNS1-deficient mice revealed by haematoxylin and eosin staining of small intestine from 9–12-month-old CNS1^{-} (bottom and right) and littermate control mice (top). An early crypt abscess is indicated (asterisk). Data are representative of ≥20 mice analysed. **c**, Percentage of Foxp3^{+} CD4^{+} cells expressing Gata3^{+} in 3-month-old mice. **d**, Percentage of total 16S rRNA gene sequences of the Firmicutes and Bacteroidetes phyla in stool from individually housed CNS1^{-} ($n = 9$) and WT ($n = 6$) littermate mice. All data are representative of three or more independent experiments with ≥3 mice per group. Error bars show s.d. (**a**, **c**) or s.e.m. (**d**). *$P < 0.05$, **$P < 0.01$, ***$P < 0.001$, as calculated by Student's *t*-test. Scale bars, 150 μm.

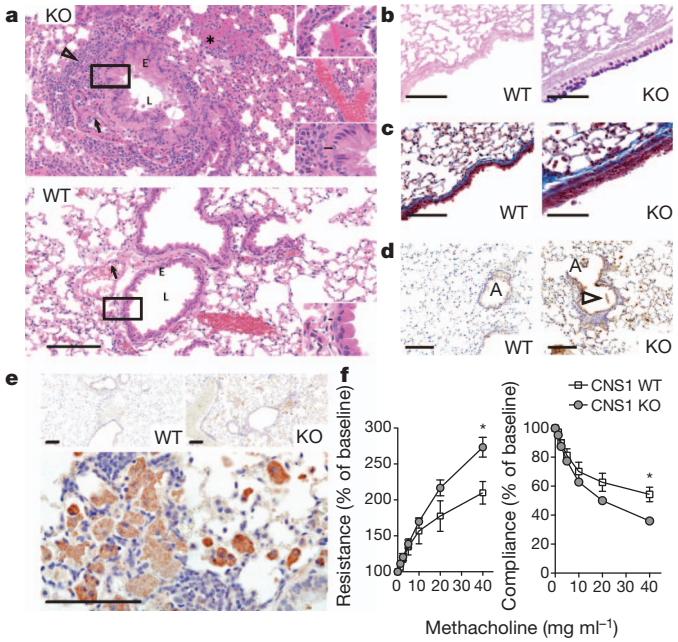

Figure 4 | Unprovoked asthma-like airway pathology in CNS1-deficient mice. **a**, Representative haematoxylin and eosin-stained lung sections from CNS1$^-$ (top) and WT (bottom) mice. The CNS1$^-$ lung has marked peribronchiolar inflammation (arrowhead). The reduced lumen (L) contains mucus produced by the hyperplastic respiratory epithelium (E). Arrows indicate reactive (top) and normal (bottom) endothelium. Bottom right hand corner insets are higher magnification of boxed regions and bar indicates smooth muscle thickness. Top right inset (KO) demonstrates eosinophilic crystals. Asterisk marks acidophilic macrophages. **b**, Periodic acid Schiff with Alcian Blue staining highlighting mucus-producing goblet cells (dark blue-purple) **c**, Trichrome staining illustrating lung fibrosis (blue staining). **d**, Arginase-1 staining of lungs from CNS1$^-$ and WT mice. A indicates airway; an acidophilic crystal is marked by the arrowhead. **e**, Chitinase 3-like 3 (Chi3l3) staining of lungs from CNS1$^-$ and WT mice at 10× magnification (top) and 60× magnification of lungs from CNS1$^-$ mice demonstrating robust Chi3l3 expression within acidophilic macrophages (bottom). **f**, Lung resistance (left) and compliance (right) of CNS1$^-$ and WT littermate control mice after exposure to methacholine. Data representative of two independent experiments with ≥4 mice per group. Error bars, s.d.; $*P < 0.05$, $**P < 0.01$, $***P < 0.001$, as calculated by Students' *t*-test. Scale bars, 100 μm.

also contributes to the local cytokine environment, which facilitates iT$_{reg}$ cell differentiation and maintenance in the gut[1]. These observations raise a question as to whether iT$_{reg}$ cells, in turn, influence composition of the commensal microbiota. To address this question, we sequenced 16S ribosomal RNA coding genes from bacterial contents of stool samples isolated from CNS1$^-$ and CNS1^{WT} littermates, which were housed individually for 5 weeks after weaning. Phylogenetic analysis revealed distinct gut microbial communities in CNS1$^-$ mice, with statistically significant enrichment of the candidate phylum TM7 and the genus Bacteroidetes *Alistipes* (Supplementary Fig. 16), and an overall decrease in the ratio of Firmicutes to Bacteroidetes (2.60 in wild-type and 1.51 in knockout) (Fig. 3d). Interestingly, an opposite trend in the Firmicutes/Bacteroidetes ratio was correlated with obesity[30], suggesting the possibility that alterations in energy harvest and metabolism (caused by inflammation or microbe-dependent effects on energy balance) could account for the decreased weight observed in iT$_{reg}$ cell deficient mice. Thus, iT$_{reg}$ cells help maintain a 'normal' microbial community in the gut, probably through exerting control over T$_H$2 mucosal inflammation.

These observations raised the question of whether the altered microbiota, rather than iT$_{reg}$ deficiency, was the direct cause of observed T$_H$2 inflammation. To equalize gut microbiota, CNS1$^-$ and littermate controls were treated with antibiotics (metronidazole and ciprofloxacin) for 4 weeks. Despite indistinguishable microbial communities, antibiotic treatment did not lead to a decrease in Gata3 expression or Th2 cytokine production by effector T cells in CNS1$^-$ mice, and characteristic histopathologic features were maintained (Supplementary Fig. 17). Furthermore, iT$_{reg}$ cell sufficient germ-free mice colonized with CNS1$^-$ or control microbiota exhibited a similar spectrum of T$_H$1, T$_H$2 and T$_H$17 cytokine production and eventual normalization of microbiota (Supplementary Fig. 18 and data not shown). These results suggest that iT$_{reg}$ deficiency results in immune dysregulation and T$_H$2 inflammation in the gut with subsequent perturbation of the microbial community.

According to the notion of specialized iT$_{reg}$ cell function in suppression of T$_H$2 responses at mucosal sites, one would expect to observe T$_H$2-type pathology in the lungs of CNS1$^-$ mice, despite an only modest ~20–25% decrease in numbers of T$_{reg}$ cells in this tissue compared to littermate controls (Fig. 1c). Indeed, we discovered that CNS1$^-$ mice suffer from spontaneous T$_H$2-type airway inflammation (Fig. 4 and Supplementary Fig. 19). The lungs of CNS1$^-$ mice were characterized by increased infiltration by lymphocytes, plasma cells and macrophages, and by moderate neutrophil infiltration (Fig. 4). The consistent features of the chronic inflammatory airway disease observed in CNS1$^-$ mice include lymphocytic infiltration, narrowed airway lumen (Fig. 4a), increased goblet cells and mucus production (Fig. 4a and b), smooth muscle hyperplasia, and fibrosis (Fig. 4c). Notably, 9/12 CNS1$^-$ and 0/6 CNS1^{WT} mice developed acidophilic macrophage pneumonia (AMP) with characteristic increases in acidophilic macrophages and both intracellular and extracellular chitinase 3-like 3 crystals (Chi3l3, formerly Ym1), analogous to Charcott-Lyden crystals found in asthmatic patients (Fig. 4a and e). In addition, the prominent presence of alternatively activated macrophages in the lungs of CNS1$^-$ mice was confirmed by morphology and expression of arginase 1 in addition to Chi3l3 (Fig. 4d and Supplementary Fig. 20). Furthermore, both young (6–8 week old) and aged (20 week old) CNS1$^-$ mice exhibited airway hyper-responsiveness accompanied by AMP, perivascular, peribronchiolar and intramucosal inflammation, bronchial epithelial hyperplasia, and airway narrowing (Fig. 4f and Supplementary Fig. 21). These spontaneous lesions are especially striking considering the T$_H$2-resistant, T$_H$1-prone C57BL/6 genetic background of CNS1$^-$ mice. The lung pathology in CNS1$^-$ mice reflects the hallmark features of chronic allergic inflammation and asthma.

Our results demonstrate that T$_{reg}$ cells of thymic and extrathymic origin have distinct mechanistic requirements for differentiation and exert specialized functions in immune homeostasis. The restriction of lesions to mucosal tissues in iT$_{reg}$ deficient mice implies that under steady state conditions T$_{reg}$ cells generated in the thymus are largely sufficient for control of most immune responses to self-antigens. These findings suggest that in normal animals, T$_{reg}$ cells generated extrathymically in a CNS1-dependent manner play a non-redundant role in control of mucosal allergic Th2 inflammation and asthma.

METHODS SUMMARY

The generation of the following mouse strains has been previously described[5,20]: CNS1$^-$ (*Foxp3*$^{\Delta CNS1}$), *Foxp3*^{GFP} and *Foxp3*$^{eGFP\text{-}Cre\text{-}ERT2}$ R26Y. *Rag1*$^-$ mice were purchased from The Jackson Laboratory, and CD45.1 B6 and *Tcrb/Tcrd*$^-$ mice, along with above strains were maintained in the Sloan Kettering Institute Research Laboratories animal facility in accordance with institutional regulations. Tissues for histologic analysis were fixed in 10% phosphate-buffered formalin and processed routinely for staining. *In vitro* induction assays were performed with 5×10^4 Foxp3–GFP$^-$ CD4$^+$ T cells and 5 μg ml^{-1} of anti-CD3 and anti-CD28 antibody, 100 U ml^{-1} IL-2, in 96-well, flat-bottom plates. For *in vitro* and transfer experiments, CD4$^+$ T cells were pre-enriched using mouse CD4 Dynabeads (L3T4, Invitrogen) and FACS sorted on an LSR-II (BD Biosciences). Intracellular staining for IL-4 used Cytofix/Cytoperm (BD Biosciences), and staining for other cytokines, Foxp3 and Gata3, used the Foxp3 staining kit (eBiosciences). For measurement of AHR, mice were anaesthetized with pentobarbitol and AHR was assessed by invasive measurement of airway resistance using modified version of a described method (Buxco Electronics). 16S rRNA sequencing was performed on a 454 GS

FLX Titanium pyrosequencing platform following the Roche 454 recommended procedures.

Full Methods and any associated references are available in the online version of the paper at www.nature.com/nature.

Received 6 July; accepted 6 December 2011.
Published online 8 February 2012.

1. Maloy, K. J. & Powrie, F. Intestinal homeostasis and its breakdown in inflammatory bowel disease. *Nature* **474,** 298–306 (2011).
2. Sakaguchi, S., Yamaguchi, T., Nomura, T. & Ono, M. Regulatory T cells and immune tolerance. *Cell* **133,** 775–787 (2008).
3. Chen, W. *et al.* Conversion of peripheral $CD4^+CD25^-$ naive T cells to $CD4^+CD25^+$ regulatory T cells by TGF-β induction of transcription factor Foxp3. *J. Exp. Med.* **198,** 1875–1886 (2003).
4. Tone, Y. *et al.* Smad3 and NFAT cooperate to induce Foxp3 expression through its enhancer. *Nature Immunol.* **9,** 194–202 (2008).
5. Zheng, Y. *et al.* Role of conserved non-coding DNA elements in the *Foxp3* gene in regulatory T-cell fate. *Nature* **463,** 808–812 (2010).
6. Hill, J. A. *et al.* Retinoic acid enhances Foxp3 induction indirectly by relieving inhibition from $CD4^+CD44^{hi}$ cells. *Immunity* **29,** 758–770 (2008).
7. Nolting, J. *et al.* Retinoic acid can enhance conversion of naive into regulatory T cells independently of secreted cytokines. *J. Exp. Med.* **206,** 2131–2139 (2009).
8. Xu, L. *et al.* Positive and negative transcriptional regulation of the *Foxp3* gene is mediated by access and binding of the Smad3 protein to enhancer I. *Immunity* **33,** 313–325 (2010).
9. Liu, Y. *et al.* A critical function for TGF-β signaling in the development of natural $CD4^+CD25^+Foxp3^+$ regulatory T cells. *Nature Immunol.* **9,** 632–640 (2008).
10. Ouyang, W., Beckett, O., Ma, Q. & Li, M. O. Transforming growth factor-β signaling curbs thymic negative selection promoting regulatory T cell development. *Immunity* **32,** 642–653 (2010).
11. Curotto de Lafaille, M. A. & Lafaille, J. J. Natural and adaptive $foxp3^+$ regulatory T cells: more of the same or a division of labor? *Immunity* **30,** 626–635 (2009).
12. Mucida, D. *et al.* Oral tolerance in the absence of naturally occurring Tregs. *J. Clin. Invest.* **115,** 1923–1933 (2005).
13. Bautista, J. L. *et al.* Intraclonal competition limits the fate determination of regulatory T cells in the thymus. *Nature Immunol.* **10,** 610–617 (2009).
14. Leung, M. W., Shen, S. & Lafaille, J. J. TCR-dependent differentiation of thymic $Foxp3^+$ cells is limited to small clonal sizes. *J. Exp. Med.* **206,** 2121–2130 (2009).
15. Moran, A. E. *et al.* T cell receptor signal strength in Treg and iNKT cell development demonstrated by a novel fluorescent reporter mouse. *J. Exp. Med.* **208,** 1279–1289 (2011).
16. Lathrop, S. K. *et al.* Peripheral education of the immune system by colonic commensal microbiota. *Nature* **478,** 250–254 (2011).
17. Komatsu, N. *et al.* Heterogeneity of natural $Foxp3^+$ T cells: a committed regulatory T-cell lineage and an uncommitted minor population retaining plasticity. *Proc. Natl Acad. Sci. USA* **106,** 1903–1908 (2009).
18. Hori, S. Regulatory T cell plasticity: beyond the controversies. *Trends Immunol.* **32,** 295–300 (2011).
19. Zhou, X. *et al.* Instability of the transcription factor Foxp3 leads to the generation of pathogenic memory T cells *in vivo*. *Nature Immunol.* **10,** 1000–1007 (2009).
20. Rubtsov, Y. P. *et al.* Stability of the regulatory T cell lineage *in vivo*. *Science* **329,** 1667–1671 (2010).
21. Josefowicz, S. Z. & Rudensky, A. Control of regulatory T cell lineage commitment and maintenance. *Immunity* **30,** 616–625 (2009).
22. Gottschalk, R. A., Corse, E. & Allison, J. P. TCR ligand density and affinity determine peripheral induction of Foxp3 *in vivo*. *J. Exp. Med.* **207,** 1701–1711 (2010).
23. Kretschmer, K. *et al.* Inducing and expanding regulatory T cell populations by foreign antigen. *Nature Immunol.* **6,** 1219–1227 (2005).
24. Tian, L. *et al.* Foxp3 regulatory T cells exert asymmetric control over murine helper responses by inducing Th2 cell apoptosis. *Blood* **118,** 1845–1853 (2011).
25. Chaudhry, A. *et al.* $CD4^+$ regulatory T cells control T_H17 responses in a Stat3-dependent manner. *Science* **326,** 986–991 (2009).
26. Koch, M. A. *et al.* The transcription factor T-bet controls regulatory T cell homeostasis and function during type 1 inflammation. *Nature Immunol.* **10,** 595–602 (2009).
27. Zheng, Y. *et al.* Regulatory T-cell suppressor program co-opts transcription factor IRF4 to control T_H2 responses. *Nature* **458,** 351–356 (2009).
28. Wang, Y., Su, M. A. & Wan, Y. Y. An essential role of the transcription factor GATA-3 for the function of regulatory T cells. *Immunity* **35,** 337–348 (2011).
29. Wohlfert, E. A. *et al.* GATA3 controls $Foxp3^+$ regulatory T cell fate during inflammation in mice. *J. Clin. Invest.* **121,** 4503–4515 (2011).
30. Turnbaugh, P. J. *et al.* An obesity-associated gut microbiome with increased capacity for energy harvest. *Nature* **444,** 1027–1031 (2006).

Supplementary Information is linked to the online version of the paper at www.nature.com/nature.

Acknowledgements We thank T. Tedder for depleting CD20 antibody, R. Tudor for assistance interpreting lung pathology, P. DeRoos for assistance with Ig ELISA assays, B. Johnson for immunohistochemical expertise, Y. Chen for assistance with airway measurements, and E. Pamer, L. Lipuma, A. Gobourne and R. Khanin for help with analysis of intestinal microbiota. This work was supported by NIH MSTP grant GM07739 and NINDS grant 1F31NS073203-01 (R.E.N.), Strategic Young Researcher Overseas Visits Program for Accelerating Brain Circulation from Department of Microbiology and Immunology, Keio University School of Medicine (T.C.) and NIH grant R37 AI034206 (A.Y.R.). A.Y.R is an investigator with the Howard Hughes Medical Institute.

Author Contributions S.Z.J., R.E.N. and H.Y.K. performed experiments and analysed data, with assistance from T.C. for tissue Ig ELISA experiments, and P.T. for immunohistochemistry and histopathology analysis. D.T.U., S.Z.J., R.E.N., H.Y.K, and A.Y.R designed and interpreted AHR experiments. Y.Z. generated $CNS1^-$ mice. S.Z.J., R.E.N. and A.Y.R. designed experiments and wrote the paper.

Author Information Reprints and permissions information is available at www.nature.com/reprints. The authors declare no competing financial interests. Readers are welcome to comment on the online version of this article at www.nature.com/nature. Correspondence and requests for materials should be addressed to A.Y.R. (rudenska@mskcc.org).

METHODS

Mice. The generation of the following mouse strains has been previously described[5,20]: CNS1^{-} (*Foxp3*$^{\Delta CNS1}$), *Foxp3*^{GFP} and *Foxp3*$^{eGFP\text{-}Cre\text{-}ERT2}$ R26Y. *Rag1*$^{-}$ mice were purchased from The Jackson Laboratory, and CD45.1 B6 and *Tcrb/Tcrd*$^{-/-}$ mice, along with above strains were maintained in the Sloan Kettering Institute Research Laboratories animal facility in accordance with institutional regulations. Mice were killed by CO_2 asphyxiation. EAE was induced and scored as previously described[31]. For antibiotic treatment, CNS1-deficient and sufficient mice were treated with 1 g l^{-1} metronidazole (Sigma-Aldrich) and 0.2 g l^{-1} ciprofloxacin (ENZO Life Sciences International) dissolved in drinking water for 4 weeks. Mouse anti-CD20[8] (MB20-11, provided by T. Tedder) and anti-IL-4 (11b.11, NCI-Frederick) were administered weekly as intraperitoneal injections of 50 μg or 5 μg, respectively, for 3 weeks.

Cell isolation, transfer and FACS staining. For *in vitro* and *in vivo* transfer experiments, CD4^{+} T cells were pre-enriched using mouse CD4 Dynabeads (L3T4, Invitrogen) and FACS sorted on an LSR-II (BD Biosciences). Intracellular staining for IL-4 used Cytofix/Cytoperm following treatment with Golgi-Stop (BD Biosciences), and staining for other cytokines (following treatment with Golgi-Plug, BD Biosciences) and Foxp3 and Gata3 used the Foxp3 staining kit (eBiosciences).

***In vitro* assays.** *In vitro* induction assays were performed with 5×10^4 Foxp3–GFP^{-} CD4^{+} T cells and 5 μg ml^{-1} of anti-CD3 and anti-CD28 antibody, 100 U ml^{-1} IL-2, in 96-well, flat-bottom plates. For *in vitro* suppression assays, 4×10^4 CD4^{+}Foxp3^{-}CD62L^{high} naive T cells FACS purified from WT mice were cultured with graded numbers of CD4^{+}Foxp3^{+} T$_{reg}$ cells FACS purified from *Foxp3*$^{\Delta CNS1}$ or *Foxp3*^{gfp} mice in the presence of 10^5 irradiated T cell-depleted splenocytes and 1 μg ml^{-1} anti-CD3 antibody in a 96-well round-bottom plate for 80 h. Cell proliferation was assessed by [^{3}H]thymidine incorporation during the final 8 h of culture.

Histology and immunohistochemistry. Necropsies were performed, and sections of pancreas, stomach, heart, lungs, kidney, external ear and haired skin were fixed in 10% phosphate-buffered formalin. Tissues were processed routinely for staining with haematoxylin and eosin, periodic acid Schiff with Alcian blue or Masson Trichrome if indicated. Slides were examined by an American Board of Veterinary Practitioners-certified veterinary pathologist blinded to genotypes. Morphological diagnoses were applied for all tissues. Immunohistochemical staining was performed by the University of Washington Histology and Imaging Core using standard protocols with a Leica Bond Automated Immunostainer. Primary antibodies: goat anti-mouse chitinase 3-like 3/ECF-L (YM1) (R&D systems, cat. no. AF2446, lot no. UNU01), 0.2 μg ml^{-1}; rabbit polyclonal anti iNOS/NOS II, NT (Millipore, cat. no. 06-573), 1 μg ml^{-1}; rabbit polyclonal anti arginase 1 (H-52) (Santa Cruz, cat. no. sc-20150, lot no. K0807), 0.2 μg ml^{-1}. Isotype controls were used at the same concentration as the primary antibody with all antibodies run with Lecia Bond reagents and Bond Polymer Refine (DAB) detection with haematoxylin counter stain.

Histology inflammation scoring. 0, None; 1, focal or multifocal mild perivascular accumulations with minimal extension into surrounding adventia or parenchyma; 2, multifocal mild or focal moderate perivascular accumulations with mild extension into surrounding parenchyma or mild to moderate parenchymal accumulations; 3, grade 2 plus mild inflammation-associated parenchymal lesions such as loss or degeneration of cells; 4, grade 2 plus moderate to severe inflammation-associated parenchymal lesions. Inflammation in the gastrointestinal tract was scored as described previously[32].

Airway hyperresponsiveness measurements. For measurement of AHR, mice were anaesthetized with pentobarbitol (7.5–10 mg per mouse) and AHR was assessed by invasive measurement of airway resistance using modified version of a described method (Buxco Electronics). Mice were ventilated at a tidal volume of 0.2 ml with the use of a ventilator (Harvard Apparatus) and frequency was set around 150 Hz. Baseline pulmonary mechanics and responses to ventilated saline (0.9% NaCl) were measured, and lung resistance (R_L) was measured in response to increasing doses (0.125–40 mg ml^{-1}) of acetyl-β-methylcholine chloride (methacholine; MCh) (Sigma-Aldrich). The three values of R_L obtained after each dose of methacholine were averaged to obtain the final values for each dose. Results are expressed as percentage of increase of saline-baseline. Following measurement of AHR, mouse tracheas were cannulated and the lungs were lavaged twice with 1 ml of PBS 2% FCS and the fluids were pooled. Cells in the lavage fluid were counted using a haemocytometer, and BAL cell differential counts were determined on slide preparations stained with DiffQuik. At least 200 cells were differentiated on stained slides by light microscopy using conventional morphological criteria. For some experiments, BAL for each mouse or grouped BAL was stained and analysed by flow cytometry.

Stool sample collection. Fresh stool samples were induced directly into sterile collection tubes from live CNS1^{-} and control mice and snap frozen before preparation of material for sequencing (see below).

DNA extraction. DNA extraction was performed on each fecal specimen using phenol-chloroform extraction with mechanical disruption based on a previously described protocol[33] Briefly, an aliquot (~500 mg) of each sample was suspended in a solution containing 500 μl of extraction buffer (200 mM Tris, pH 8.0; 200 mM NaCl; and 20 mM EDTA), 210 μl of 20% SDS, 500 μl of phenol/chloroform/isoamyl alcohol (25:24:1), and 500 μl of 0.1-mm-diameter zirconia/silica beads (BioSpec Products). Microbial cells were lysed by mechanical disruption with a bead beater (BioSpec Products) for 2 min, after which two rounds of phenol/chloroform/isoamyl alcohol extraction were performed. DNA was precipitated with ethanol and resuspended in 50 μl of nuclease-free water. DNA was subjected to additional purification with the QIAamp DNA Mini Kit (Qiagen).

PCR amplification and sequencing. For each sample, three replicate 25 μl PCR amplifications were performed, each containing 5 ng of purified DNA, 0.2 mM dNTPs, 1.5 mM $MgCl_2$, 1.25 U Platinum Taq DNA polymerase, 2.5 μl of 10× PCR buffer, and 0.2 μM each of broad-range bacterial forward and reverse primers as described previously[34], flanking the V1–V3 variable region. The primers were modified to include adaptor sequences required for 454 sequencing, with the addition of a unique 6–8 base barcode in the reverse primer. The forward primer (5′-CCTATCCCCTGTGTGCCTTGGCAGTCTC*AGAGTTTGATCCTGGCTCAG*-3′) consisted of the 454 Lib-L primer B (underlined) and the broad-range universal bacterial primer 8F (italics); the reverse primer (5′-CCATCTCATCCCTGCGTGTCTCCGACTCAGNNNNNNN*ATTACCGCGGCTGCTGG*-3′) consisted of the 454 Lib-L primer A, barcode (NNNNNNN), and the broad-range primer 534R (italics). The cycling conditions were: 94 °C for 3 min, then 25 cycles of 94 °C for 30 s, 56 °C for 30 s, and 72 °C for 1 min. The three replicate PCR products were pooled and subsequently purified using the Qiaquick PCR Purification Kit (Qiagen). The purified PCR products were sequenced unidirectionally on a 454 GS FLX Titanium pyrosequencing platform following the Roche 454 recommended procedures.

Sequence processing and analysis. Sequences were converted to standard FASTA format using Vendor 454 software. Sequences shorter than 200 base pairs (bp), containing undetermined bases or homopolymer stretches longer than 8 bp, or failing to align with the V1–V3 region were excluded from the analysis. Using the 454 base quality scores, which range from 0 to 40 (0 being an ambiguous base), sequences were trimmed using a sliding-window technique, such that the minimum average quality score over a window of 50 bases never dropped below 35. Sequences were trimmed from the 3′-end until this criterion was met. Sequences were aligned to the V1–V3 region of the 16S gene, using as template the SILVA reference alignment[35] and the Needleman-Wunsch algorithm with default scoring options. Potentially chimaeric sequences were removed using the chimaera uchime program[36]. Sequences were grouped into operational taxonomic units (OTUs) using the average neighbour algorithm. Sequences with distance-based similarity of 97% or greater were assigned to the same OTU. For each fecal sample, OTU-based microbial diversity was estimated by calculating the Shannon diversity index[37]. Phylogenetic classification to genus level was performed for each sequence, using the Bayesian classifier algorithm described by Wang and colleagues, using a database of known 16S sequences generated by the Ribosomal Database Project (RDP)[38]. For each experiment, data were analysed on each taxon level individually. The count data was rescaled using DESeq R package[39]. Bacteria with less than 10 mean count in both conditions were removed from further analysis and bacteria with statistically significant differences between two conditions (for example, WT and KO), were determined using binomial test (from DESeq package). Bacteria with fold-change greater than two and FDR = 0.05 were declared significant.

31. Stromnes, I. M. & Goverman, J. M. Active induction of experimental allergic encephalomyelitis. *Nature Protocols* **1,** 1810–1819 (2006).
32. Burich, A. *et al.* Helicobacter-induced inflammatory bowel disease in IL-10- and T cell-deficient mice. *Am. J. Physiol. Gastrointest. Liver Physiol.* **281,** G764–G778 (2001).
33. Ubeda, C. *et al.* Vancomycin-resistant Enterococcus domination of intestinal microbiota is enabled by antibiotic treatment in mice and precedes bloodstream invasion in humans. *J. Clin. Invest.* **120,** 4332–4341 (2010).
34. Nossa, C. W. *et al.* Design of 16S rRNA gene primers for 454 pyrosequencing of the human foregut microbiome. *World J. Gastroenterol.* **16,** 4135–4144 (2010).
35. Schloss, P. D. *et al.* Introducing mothur: open-source, platform-independent, community-supported software for describing and comparing microbial communities. *Appl. Environ. Microbiol.* **75,** 7537–7541 (2009).
36. Edgar, R. C. *et al.* UCHIME improves sensitivity and speed of chimera detection. *Bioinformatics* **27,** 2194–2200 (2011).
37. Magurran, A. E. *Measuring Biological Diversity* (Blackwell, 2004).
38. Wang, Q. *et al.* Naive Bayesian classifier for rapid assignment of rRNA sequences into the new bacterial taxonomy. *Appl. Environ. Microbiol.* **73,** 5261–5267 (2007).
39. Anders, S. & Huber, W. Differential expression analysis for sequence count data. *Genome Biol.* **11,** R106 (2010).